IVYSPRING INTERNATIONAL PUBLISHER

International Journal of Biological Sciences

2027; 23(1): 59-76. doi: 10.7150/ijbs.136182

Research Paper

TRPP2 Drives Anti-PD-1 Resistance in Head and Neck Cancer by Stabilizing PD-L1 and Promoting Its Exosomal Export

Ziqi Meng[1,2,3*], Xu Huang[2*], Jinjie Wang[1,4*], Jiyuan Shi[5], Yuxin Zhang[4], Suwen Bai[6], Xinyue Zhang[3], Minghua Wang[1], Zhenye Yang[7], Xiaoqiang Yao[8], Xu Ji[9], Juan Du[1,3,10]✉

1. The Second Affiliated Hospital, School of Medicine, The Chinese University of Hong Kong, Shenzhen & Longgang District People's Hospital of Shenzhen, Shenzhen, 518172, China.
2. Longgang Central Hospital of Shenzhen, Shenzhen, 518116, China.
3. School of Medicine, The Chinese University of Hong Kong, Shenzhen, Guangdong, 518172, China.
4. School of Basic Medical Sciences, Anhui Medical University, Hefei, Anhui, 230032, China.
5. West China Xiamen Hospital, Sichuan University, Xiamen, Fujian, 361022, China.
6. Shenzhen Longgang Otolaryngology hospital & Shenzhen Otolaryngology Research Institute, 518172, China.
7. Key Laboratory of Immune Response and Immunotherapy, Division of Life Sciences and Medicine, University of Science and Technology of China, Hefei, Anhui, 230027, China.
8. School of Biomedical Sciences, The Chinese University of Hong Kong, Shatin, Hong Kong, China.
9. The First Affiliated Hospital of China Medical University, Shenyang, 110001, China.
10. Guangdong Basic Research Center of Excellence for Aggregate Science, School of Science and Engineering, The Chinese University of Hong Kong, Shenzhen, Guangdong, 518172, China.

*These authors contributed equally and were considered co-first authors.

✉ Corresponding author: Juan Du, Ph.D., School of Medicine, The Chinese University of Hong Kong, Shenzhen, 2001 Longxiang Road, Longgang District, Shenzhen, Guangdong, P. R. of China 518172; Tel.: +86-755-23516109; dujuan@cuhk.edu.cn.

© 2027 The Author(s). This is an open access article distributed under the Creative Commons Attribution 4.0 International Licence, subject to the Publisher's Terms of Use at https://ivyspring.com/terms.

Received: 2026.04.14; Accepted: 2026.09.07; Published: 2027.01.01

Abstract

The infiltration of immunosuppressive cells within the tumor microenvironment (TME), along with aberrant expression of immunosuppressive factors such as programmed cell death ligand 1 (PD-L1), critically contributes to immunotherapy resistance and collectively drives tumor immune evasion. Although Transient Receptor Potential Polycystic 2 (TRPP2) has been implicated in the malignant progression of head and neck cancer (HNC), its specific role in shaping the tumor immune microenvironment (TIME) and its impact on the efficacy of HNC immunotherapy remain unclear. In this study, TRPP2 was found to be upregulated in HNC tissues, and its expression levels positively correlated with PD-L1 expression, the infiltration densities of tumor-associated macrophages (TAMs) and myeloid-derived suppressor cells (MDSCs), as well as the exhaustion of $CD8^+$T cells. Mechanistically, TRPP2 enhanced ubiquitin-specific peptidase 10 (USP10)-mediated deubiquitination of PD-L1 in HNC cells, while concurrently promoting the sorting of PD-L1 into exosomes via upregulation of HRS. Upon secretion into the TME, these exosomes directly suppressed $CD8^+$T cells through membrane-bound PD-L1 and also transferred PD-L1 to TAMs, inducing their M2-type polarization and thereby inhibiting $CD8^+$T cell function. Based on these findings, targeting TRPP2 in combination with anti-programmed cell death protein 1 (PD-1) monoclonal antibody (mAb) therapy reduced immunosuppressive cell infiltration and restored $CD8^+$T cell activity, leading to significant tumor growth inhibition in a mouse model of HNC. Collectively, this study elucidates the molecular mechanism by which TRPP2 induces $CD8^+$T cell immunosuppression through enhancing PD-L1 protein stability and promoting its exosomal export, suggesting that targeting TRPP2 represents a promising strategy to enhance the sensitivity of HNC to anti-PD-1 mAb therapy.

Keywords: head and neck cancer, TRPP2, PD-L1, exosome, immunotherapy resistance

Introduction

Head and neck cancer (HNC) is characterized by marked invasiveness and an insidious clinical course, with the majority of patients presenting at advanced or metastatic stages [1]. Despite aggressive multimodal

intervention, recurrence rates remain high and five-year survival rate remains below 50% [2, 3]. Although immune checkpoint inhibitors (ICIs) targeting the PD-1/PD-L1 axis have been approved as first-line therapy for recurrent or metastatic HNC, the objective response rate remains disappointingly low at approximately 15%, largely attributable to profound tumor heterogeneity and a deeply immuno suppressive tumor microenvironment (TME) [4, 5]. Consequently, delineating the molecular networks that govern immune evasion in HNC and identifying actionable targets to overcome ICI resistance represents a pressing clinical priority.

PD-L1 expression on both tumor and host cells serves as a pivotal biomarker for predicting ICI efficacy [6]. Notably, PD-L1-driven immunosuppression extends beyond direct cell-cell contact. Emerging evidence demonstrates that tumor-derived exosomal PD-L1 acts as a systemic mediator of immune subversion [7, 8]. These extracellular vesicles (30-150 nm in diameter) not only deliver PD-L1 to neighboring stromal and immune cells within the TME, thereby sculpting a pro-tumor landscape, but also evade therapeutic antibody blockade, leading to persistent T-cell exhaustion [9-13]. Despite its biological significance, the upstream molecular circuitry controlling intracellular PD-L1 protein stability and its subsequent sorting into exosomes remains poorly defined.

Transient Receptor Potential Polycystic 2 (TRPP2), a non-selective cation channel predominantly localized to the endoplasmic reticulum, functions as a master regulator of intracellular calcium homeostasis [14]. Previous studies have established TRPP2 as an oncogenic driver that fuels malignant progression via calcium-dependent signaling in various cancers [15, 16]. Notably, precise calcium signaling is also a fundamental determinant of multivesicular body (MVB) biogenesis and exosome secretion [17, 18]. Building on this biological premise, we observed that TRPP2 markedly enhances exosome secretion in HNC cells. Collectively, these observations position TRPP2 at a critical signaling nexus that couples intracellular calcium dynamics with extracellular vesicle communication, suggesting an uncharacterized role in exosome-mediated immune regulation.

In this study, we hypothesized that TRPP2 remodels the immune landscape of HNC by driving the biogenesis of PD-L1-enriched exosomes. We systematically delineated a previously unrecognized TRPP2-orchestrated signaling cascade: TRPP2 not only recruits the deubiquitinase USP10 to enhance PD-L1 protein stability, but also upregulates hepatocyte growth factor-regulated tyrosine kinase substrate (HRS), a core component of the endosomal sorting complexes required for transport-0 (ESCRT-0) complex that serves as the initial sorting machinery for exosomal cargo, capturing specific cargo proteins on endosomal membranes and sorting them into intraluminal vesicles (ILVs) within MVBs, thereby initiating exosomal loading [19, 20]. Given that ESCRT-0-mediated cargo sorting is a rate-limiting step in exosomal cargo sorting, and among its core components (HRS and STAM), only HRS was significantly regulated by TRPP2, we focused on the TRPP2-HRS axis to investigate how it facilitates the precise sorting of PD-L1 into exosomes. These exported vesicles directly exert immunosuppressive activity and are taken up by macrophages to induce M2 polarization, ultimately conferring resistance to anti-PD-1 therapy. Our findings expand the biological purview of TRPP2 in tumor immunology and provide a robust rationale for targeting the TRPP2-exosomal PD-L1 axis as a strategy to sensitize HNC to immunotherapy.

Material and Methods

Cell culture

Human HNC cell lines (FaDu and Detroit562), the murine HNC cell line SCC7, and the human monocytic cell line THP-1 were obtained from the American Type Culture Collection (ATCC). All cell lines were authenticated by short tandem repeat (STR) profiling and tested negative for mycoplasma contamination. Cells were cultured in RPMI-1640 or DMEM (Gibco, USA) supplemented with 10% fetal bovine serum (FBS; Gibco, USA) and 1% penicillin-streptomycin at 37 ℃ in a humidified atmosphere containing 5% CO_2. THP-1 monocytes were differentiated into macrophages by treatment with 100 ng/mL phorbol-12-myristate 13-acetate (PMA; Sigma-Aldrich, USA) for 24 h.

Plasmid construction, lentiviral transduction, and transfection

All lentiviral particles were produced in HEK293T packaging cells by co-transfecting the respective transfer plasmids with packaging plasmid mixes provided by the manufacturers. Viral supernatants were harvested 48 h post-transfection, filtered through 0.45 μm filters, and used to transduce target cells at a MOI of 20 in the presence of polybrene (8 μg/mL). Stable transductants were selected with puromycin (2 μg/mL) for 72 h, and knockdown/overexpression efficiency was validated by Western blotting.

For human USP10 overexpression, lentiviral constructs were obtained from Beijing Syngentech Co., LTD. The overexpression vector was pLV-hef1a-

mNeongreen-P2A-Puro-WPRE-CMV-USP10-3flag and the empty vector control was pLV-hef1a-mNeongreen-P2A-Puro-WPRE-CMV-MCS-3flag. These constructs were transduced into human HNC cells.

For human TRPP2 overexpression and knockdown, lentiviral constructs were obtained from OBiO Technology Corp (Shanghai, China). The TRPP2 overexpression vector was pSLenti-CMV-TRPP2-3xFLAG-PGK-Puro-WPRE, with pSLenti-CMV-MCS-3xFLAG-PGK-Puro-WPRE as the empty vector control. The TRPP2 knockdown vector was pCLenti-U6-shRNA(TRPP2)-CMV-Puro-WPRE, with pCLenti-U6-shRNA(NC)-CMV-Puro-WPRE as the non-targeting control. These constructs were transduced into human HNC cells.

For murine TRPP2 knockdown, lentiviral constructs were also obtained from Beijing Syngentech Co., LTD. The targeting vector was pLV-hU6-shRNA (mouse TRPP2)-hef1a-mNeongreen-P2A-Puro (targeting mouse TRPP2), and the non-targeting control was pLV-hU6-shRNA(NC)-hef1a-mNeongreen-P2A-Puro. These constructs were transduced into mouse SCC7 cells.

For transient knockdown of HRS, small interfering RNAs (siRNAs) targeting HRS (siHRS#1, #2, #3) or non-targeting control siRNAs were transfected into HNC cells using Lipofectamine 3000 (Invitrogen, USA) at 5 μL per well in 6-well plates, following the manufacturer's protocol. siRNA sequences are provided in **Table S1**.

Exosome isolation and characterization

Isolation from cell supernatants: Exosomes were isolated by differential ultracentrifugation. Briefly, cell supernatants were sequentially centrifuged at 300 g for 5 min, 1000 g for 20 min and 10000 g for 30 min to remove cells and debris. The clarified supernatant was filtered through a 0.22 μm membrane and ultracentrifuged at 160000 g for 120 min. The resulting exosome pellet was resuspended in PBS and stored at -80 ℃. Exosomes were validated by TEM, NTA, and western blotting. For functional assays, exosomes were quantified by BCA protein assay and equal amounts of exosomal protein (30 μg) were added to recipient cells.

Isolation from plasma: 1 mL of whole blood was collected from mice and human subjects in the indicated treatment groups and centrifuged at 3000 rpm for 10 min. Plasma exosomes were extracted using a commercial exosome isolation kit (Absin, China).

Transmission electron microscopy (TEM)

Isolated exosomes were fixed with 2.5% glutaraldehyde and applied to copper grids. After air drying, samples were negatively stained with 10 μL of 2% phosphotungstic acid (pH=6.5) for 2 min at RT. Morphological analysis was performed using a TEM (Hitachi, Japan) operated at 120 kV.

Nanoflow cytometric analysis

Exosomes were diluted 1:100 in PBS and incubated with FITC-CD9, FITC-CD63, or APC-PD-L1 (Biolegend, USA) at 37 ℃ for 1 h. Unbound antibodies were removed using an EXODUS system (Huxin lifetech, China). Particle concentration, size distribution and the proportion of positively stained exosomes were analyzed using a nanoflow cytometer.

Exosome uptake and PD-1 binding assays

For uptake studies, exosomes were labeled with PKH26 (Sigma-Aldrich, USA) and incubated with recipient macrophages for 12 h. Internalization was visualized using a laser scanning confocal microscope (Leica, Germany). To assess PD-1 binding, 96-well plates were coated with human PD-1-Fc fusion protein (5 μg/mL; Sigma-Aldrich, USA) or BSA (negative control). PKH26-labeled exosomes were added and incubated for 2 h at RT. After three washes with PBS, binding affinity was quantified by fluorescence intensity measurement and confocal imaging.

Enzyme-linked immunosorbent assay (ELISA)

To detect PD-L1 on the surface of intact exosomes, 96-well ELISA plates were coated with a PD-L1 capture antibody (0.25 μg/well, clone 5H1-A3; Sigma-Aldrich, USA) overnight at 4 ℃. After blocking with 200 μL blocking buffer for 1 h at RT, intact exosome samples were added to assess membrane-bound PD-L1 enrichment. For quantitative evaluation of exosomal PD-L1 binding to PD-1, captured exosomes were incubated with biotinylated human PD-1 protein (4 μg/mL; BPS Bioscience, USA) for 2 h at RT, followed by HRP-conjugated streptavidin (Solarbio, China) for 1 h. Chromogenic signals were developed using tetramethylbenzidine and terminated with 0.5 N H_2SO_4. Absorbance was measured at 450 nm using a BioTek microplate reader. Recombinant human PD-L1 protein directly coated on the plate served as a positive control.

Flow cytometry (FC)

For cultured cells: Cells (1×10^6) were harvested and incubated with Fc receptor blocking solution (BD Biosciences, USA) on ice for 15 min. Surface staining was performed with APC-PD-L1 antibody at 4 ℃ for 30 min. Cells were then fixed and permeabilized, followed by intracellular staining with PE-CD206 antibody at 4 ℃ for 1 h.

For tumor tissues: tumors were dissociated into single-cell suspensions using a commercial tissue dissociation kit (Absin, China). Immune cells were enriched by Percoll density gradient centrifugation. Cells were stimulated with Cell Stimulation Cocktail (BD Biosciences, USA) at 37 °C for 6 h. Following live/dead staining and Fc receptor blockade, cells were stained with a panel of surface antibodies for 30 min at 4 °C. After fixation and permeabilization, intracellular staining was performed for 1 h at 4 °C. Samples were acquired on a Beckman flow cytometer. Antibody details are listed in **Table S2**.

Western blotting

Total protein was extracted using RIPA lysis buffer containing 1% PMSF (CWBio, China). Protein concentrations were determined by BCA assay (CWBio, China). Equal amounts of protein (20 μg per lane) were separated by SDS-PAGE and transferred to PVDF membranes (Millipore, USA). Membranes were blocked with 5% non-fat milk for 1 h, incubated with primary antibodies overnight at 4 °C, and then probed with HRP-conjugated secondary antibodies for 1 h at RT. Signals were detected using ECL reagent (ZOMANBIO, China). Antibody specifications are listed in **Table S2**.

RT-qPCR

Total RNA was extracted, reverse-transcribed into cDNA, and quantified by SYBR Green-based qPCR (Agbio Biotechnology, China). GAPDH served as the internal control. Relative mRNA expression levels were calculated using the $2^{-\Delta\Delta Ct}$ method. Primer sequences are listed in **Table S3**.

Immunofluorescence (IF) staining

Cells were fixed with ice-cold methanol for 15 min, permeabilized with 0.5% Triton X-100, and blocked with 3% BSA. Samples were incubated with primary antibodies overnight at 4 °C, followed by Alexa Fluor-conjugated secondary antibodies for 2 h at RT. Nuclei were counterstained with DAPI. Images were captured using a confocal microscope (Leica Microsystems, Germany).

Co-immunoprecipitation (Co-IP)

Cells were lysed in IP buffer. Clarified lysates were incubated with 1-3 μg of specific primary antibodies overnight at 4 °C. Protein A/G magnetic beads (25 μL; MCE, USA) were then added and incubated for 6 h at RT with rotation. Bead-protein complexes were washed, eluted in loading buffer by boiling at 95 °C for 5 min, and analyzed by western blotting.

Protein half-life assay

To determine protein half-life, HNC cells were treated with the protein synthesis inhibitor cycloheximide (CHX; 100 μg/mL) for 0, 2, 4, and 8 h. To evaluate proteasomal degradation, cells were treated with the proteasome inhibitor MG132 (10 μM) for the indicated durations. Total protein was extracted and subjected to western blotting to quantify relative PD-L1 abundance.

Ubiquitination assay

Cells were co-transfected with HA-Ub and Flag-PD-L1 plasmids. After 24 h, cells were treated with MG132 (10 μM) for 8 h. Cell lysates were prepared in IP buffer and immunoprecipitated with the indicated antibodies overnight at 4 °C, followed by incubation with Protein A/G magnetic beads. The purified complexes were resolved by western blotting to assess PD-L1 ubiquitination levels.

Animal studies

Male C3H mice (4-5 weeks old) were maintained under specific pathogen-free (SPF) conditions. Murine SCC7 cells were subcutaneously injected (5×10^5 cells in 100 μL suspension) into the axillary region. When tumor volumes reached approximately 100 mm^3, mice were randomized into four groups: (1) control+IgG, (2) TRPP2 KD+IgG, (3) control+anti-PD-1 mAb, (4) TRPP2 KD+anti-PD-1 mAb (STARTER, China). Mice received intraperitoneal injections of IgG or anti-PD-1 mAb (200 μg per dose) every three days for a total of six administrations. At the experimental endpoint, mice were euthanized and tumor volume and weight were recorded.

Immunohistochemistry (IHC)

Tumor sections were deparaffinized, rehydrated, and subjected to heat-induced antigen retrieval in citrate buffer. Endogenous peroxidase activity was blocked with 3% H_2O_2. Sections were incubated with primary antibodies overnight at 4 °C, followed by HRP-conjugated secondary antibodies. Signals were visualized using DAB chromogen (ZSGB-BIO, China), and nuclei were counterstained with hematoxylin.

Transcriptomic analysis

Total RNA was extracted using TRIzol reagent followed by DNase I digestion to remove residual DNA, with samples subsequently submitted to a commercial sequencing facility for transcriptome sequencing to assess mRNA expression profiles in THP-1 cells regulated by exosomes derived from HNC cells exhibiting differential TRPP2 expression, applying significance thresholds of $P < 0.05$ and fold

change > 1.5, while volcano plots and bubble charts were generated using R software.

Protein profiling

The cells were lysed using RIPA lysis buffer and quantified (BCA assay). Peptides were analyzed by LC-MS/MS (Q Exactive HF-X, Thermo Fisher Scientific) with a C18 column and 5–35% acetonitrile gradient. Raw data were processed using MaxQuant (UniProt database, FDR < 1%), and differentially expressed proteins (P < 0.05 and fold change > 1.5) were annotated via volcano plots.

Statistical analysis

Statistical analyses were performed using GraphPad Prism 8.0. Comparisons between two groups were evaluated using a two-tailed unpaired Student's *t*-test. For multiple group comparisons, two-way ANOVA was applied, followed by Bonferroni's post-hoc test for multiple comparisons adjustment. All experiments were independently repeated at least three times, and quantitative data are presented as mean ± SD. Adjusted P < 0.05 was considered statistically significant.

Results

TRPP2 is overexpressed in HNC and correlates with elevated PD-L1, immunosuppressive infiltration, and therapeutic resistance

Analysis of the ENCORI database revealed that TRPP2 transcript levels are significantly elevated in HNC tissues relative to adjacent normal tissues **(Fig. 1A)**. This upregulation was associated with poor overall survival **(Fig. 1B)**, supporting a potential oncogenic role for TRPP2 in HNC progression. Given the centrality of immune evasion in HNC pathogenesis, we next examined the relationship between TRPP2 and the immune checkpoint molecule PD-L1. Consistent with TRPP2 upregulation, PD-L1 expression was also markedly increased in HNC specimens and exhibited a robust positive correlation with TRPP2 levels **(Fig. 1C-D)**. We corroborated these findings in clinical HNC samples, where IF and western blotting confirmed concurrent overexpression and spatial co-localization of TRPP2 and PD-L1 **(Fig. 1E-F)**. Moreover, TIMER database profiling indicated that TRPP2 expression correlates with the infiltration of multiple immune cell subsets, predominantly those with immunosuppressive phenotypes **(Fig. 1G)**. Notably, interrogation of immunotherapy-treated cohorts (ICB and CIDE databases) revealed that TRPP2 expression was significantly higher in non-responders compared with responders **(Fig. 1H-I)**. Collectively, these clinical observations suggest that elevated TRPP2 expression contributes to an immuno suppressive TIME and facilitates resistance to immunotherapy.

TRPP2 depletion suppresses HNC progression and restores a pro-inflammatory immune microenvironment

To functionally interrogate the role of TRPP2 *in vivo*, we established subcutaneous tumors using TRPP2-knockdown murine HNC cells. Depletion of TRPP2 markedly restrained both tumor volume and weight **(Fig. 2A-B)**. IHC analysis of tumor tissues revealed that TRPP2 knockdown not only diminished PD-L1 protein levels but also attenuated tumor cell proliferation (Ki67) **(Fig. 2C)**. To semi-quantitatively evaluate these changes, we performed H-score analysis (staining intensity×percentage of positive cells) on tumor sections from each group in a blinded manner. Compared with the control group, TRPP2-knockdown tumors exhibited significantly reduced H-scores for both PD-L1 and Ki67 **(Fig. 2D)**. Pearson correlation analysis further revealed that PD-L1 H-score and Ki67 H-score were positively correlated with tumor volume (r=0.9129, P=0.0002 and r=0.9344, P<0.0001, respectively), supporting the notion that TRPP2 promotes tumor growth at least in part through upregulation of PD-L1.

FC profiling of the TIME further demonstrated that TRPP2 depletion profoundly remodels the immune landscape. In the myeloid compartment, TRPP2 knockdown significantly reduced infiltration of immunosuppressive MDSCs while increasing the proportion of anti-tumor M1-type TAMs **(Fig. S1)**. While the total abundance and proliferative fraction ($Ki67^+$) of $CD8^+$T cells remained unchanged **(Fig. 3A-C)**, their effector function was significantly restored. Specifically, TRPP2 knockdown tumors harbored increased proportions of cytotoxic ($GZMB^+$) and cytokine-secreting ($IFN\text{-}\gamma^+$) $CD8^+$T cells **(Fig. 3D-E)**, accompanied by a concomitant reduction in exhausted subsets marked by $PD\text{-}1^+$ and $TIM\text{-}3^+$ expression **(Fig. 3F-G)**. Importantly, TRPP2 depletion also diminished the immunosuppressive potency of these myeloid cells, reflected by a sharp decrease in the $CD206^+/PD\text{-}L1^+$ double-positive population **(Fig. 3H-L)**. These *in vivo* findings establish that TRPP2 maintains a PD-L1-dependent immunosuppressive barrier within the HNC microenvironment.

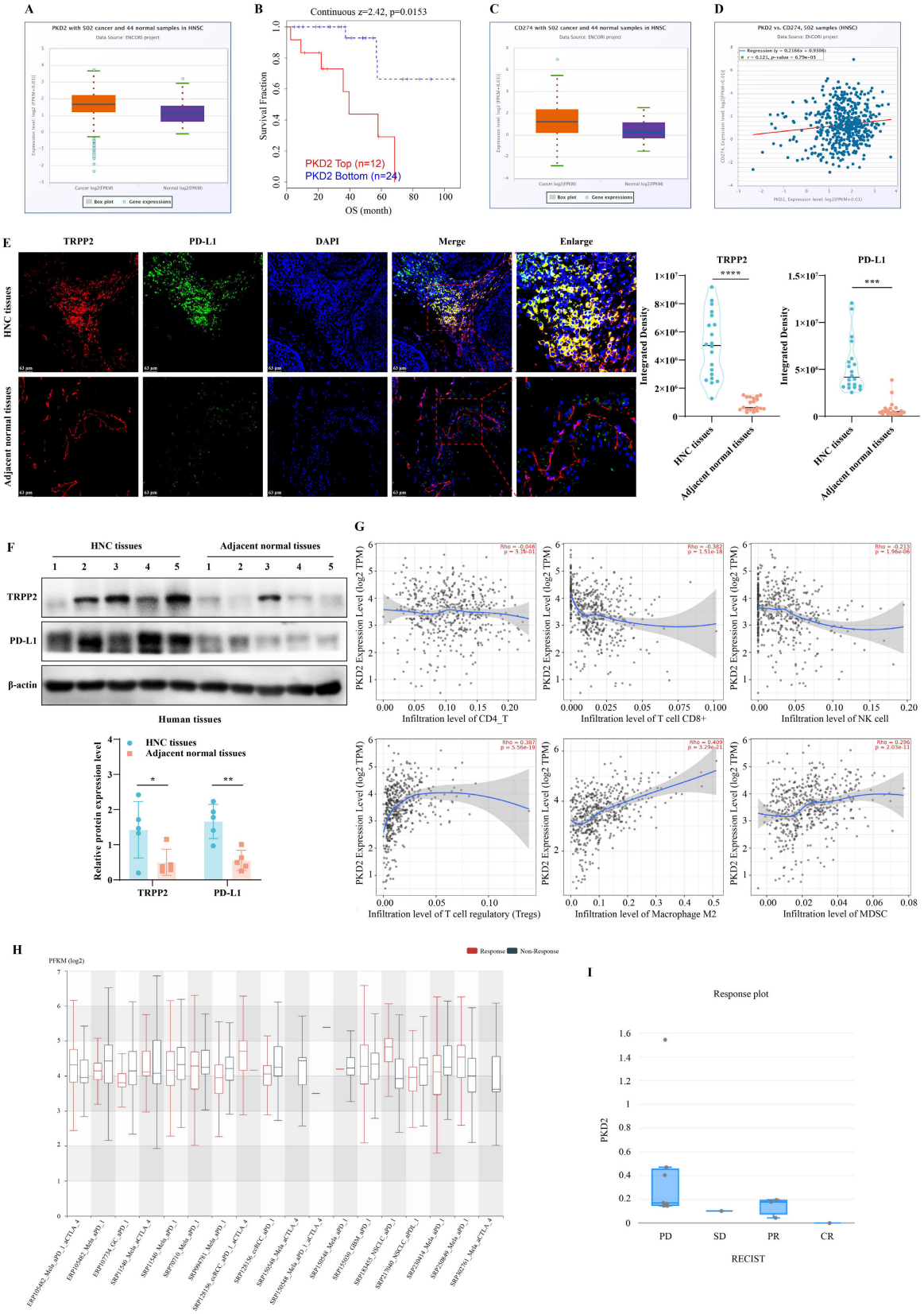


Figure 1. TRPP2 (encoded by PKD2) is overexpressed in HNC and positively correlates with PD-L1 abundance and immunotherapy resistance. (A) Expression levels of PKD2 (TRPP2) in HNC tissues versus adjacent normal tissues analyzed via the ENCORI database. **(B)** Kaplan-Meier survival analysis based on PKD2 (TRPP2) expression using the TIDE database. **(C)** PD-L1 (encoded by CD274) expression profiles in HNC cohorts retrieved from the ENCORI database. **(D)** Pearson correlation analysis between PKD2 (TRPP2) and CD274 (PD-L1) expression in HNC. **(E-F)** Representative IF and western blotting demonstrating the concurrent overexpression and spatial co-localization of TRPP2 and PD-L1 in human HNC clinical specimens compared to matched adjacent normal tissues. **(G)** Correlation between PKD2 (TRPP2) expression and immune cell infiltration profiles in HNC evaluated via the TIMER database. **(H-I)** Comparison of PKD2 (TRPP2) expression levels between immunotherapy responders and non-responders using the ICB and CIDE databases. **P*<0.05, ***P*<0.01, ****P*<0.001 and *****P*<0.0001.

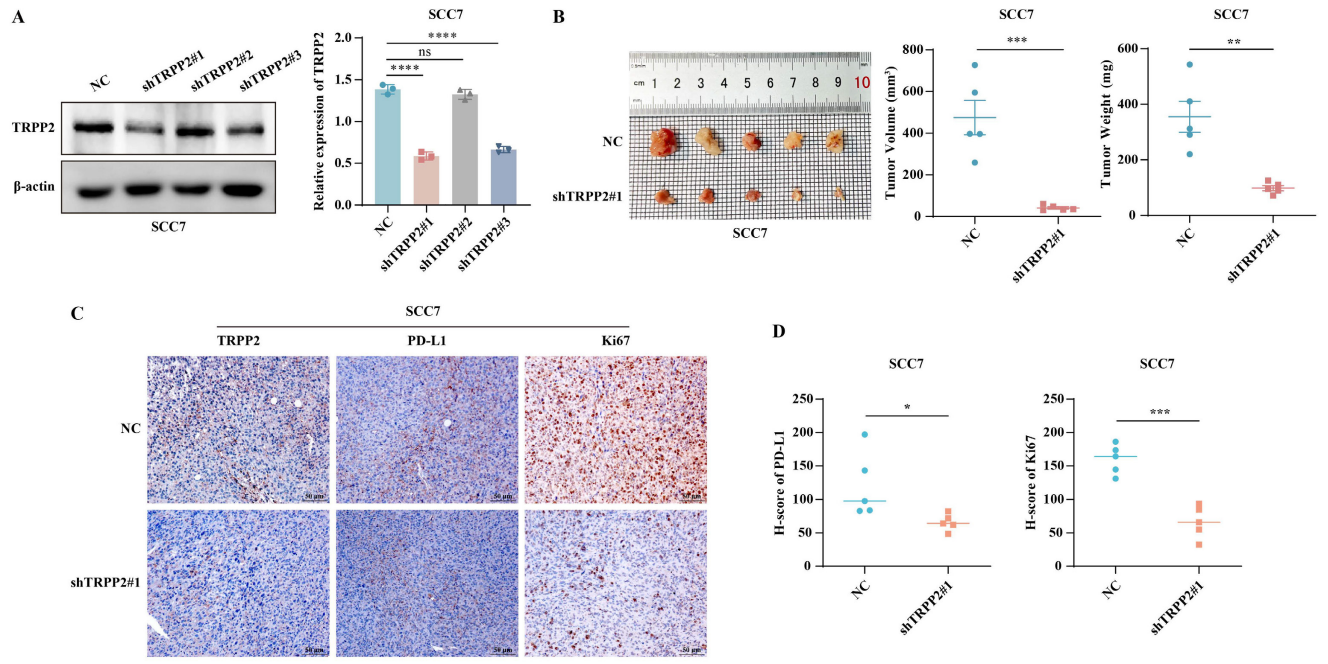


Figure 2. TRPP2 depletion restricts HNC tumor growth and malignant phenotypes *in vivo*. (A) Western blotting confirmation of TRPP2 knockdown efficiency using three distinct shRNA sequences in SCC7 cells. **(B)** Tumor growth curves (volume) and final tumor weights of mice bearing control or TRPP2-knockdown SCC7 xenografts. **(C)** Representative IHC staining images evaluating the expression of TRPP2, PD-L1, and the proliferation marker Ki67 in the xenograft tumor tissues. (D) Semi-quantitative analysis of IHC staining. H-scores of PD-L1 and Ki67 in control and TRPP2-knockdown tumor tissues (n=5 per group). **P*<0.05, ***P*<0.01, ****P*<0.001 and *****P*<0.0001. ns, not significant.

TRPP2 enhances PD-L1 protein stability via USP10-mediated deubiquitination

We next sought to delineate the molecular mechanism by which TRPP2 sustains elevated PD-L1 levels in HNC cells. Co-IP assays revealed a physical interaction between endogenous TRPP2 and PD-L1 **(Fig. 4A)**. Knockdown and overexpression experiments established that TRPP2 positively regulates PD-L1 protein levels **(Fig. 4B-C)**. RT-qPCR analysis ruled out transcriptional regulation, as PD-L1 mRNA levels were unaffected by TRPP2 manipulation **(Fig. 4D)**. IF staining and Pearson's correlation analysis revealed minimal co-localization of PD-L1 with endocytic/recycling markers (EEA1, TFRC, Rab7, Rab11, LAMP1), with no significant differences between groups, excluding altered intracellular trafficking as a primary mechanism **(Fig. 4E)**. Similarly, treatment with the lysosomal inhibitor chloroquine (CQ) did not rescue PD-L1 degradation following TRPP2 knockdown **(Fig. 4F)**. In contrast, the proteasome inhibitor MG132 effectively reversed the loss of PD-L1 induced by TRPP2 depletion **(Fig. 4G)**, and CHX chase assays demonstrated that TRPP2 overexpression significantly extended the half-life of the PD-L1 protein **(Fig. 4H)**. Ubiquitination assays further confirmed that TRPP2 knockdown increased endogenous PD-L1 polyubiquitination **(Fig. 4I)**, whereas TRPP2 overexpression reduced the ubiquitination of exogenous Flag-tagged PD-L1 **(Fig. 4J)**. Collectively, these data indicate that TRPP2 enhances PD-L1 protein stability by inhibiting its ubiquitination.

To identify the deubiquitinase responsible for this effect, we performed proteomic analysis in TRPP2-knockdown HNC cells. Among the differentially expressed proteins, only the deubiquitinase USP10 was significantly downregulated. We therefore selected USP10 for further study **(Fig. 5A)**. Co-IP assays validated the interaction between USP10 and PD-L1 in HNC cells **(Fig. 5B)**. To determine whether TRPP2 serves as an essential scaffold for the USP10-PD-L1 interaction, we performed Co-IP assays in control and TRPP2-knockdown cells with USP10 overexpression. Compared with control cells, TRPP2 knockdown markedly reduced the association between USP10 and PD-L1 **(Fig. 5C)**, indicating that TRPP2 is required for maintaining the USP10-PD-L1 interaction. Functionally, overexpression of USP10 rescued the reduction in PD-L1 protein levels, reversed the enhanced ubiquitination, and restored PD-L1 protein stability in TRPP2-silenced cells **(Fig. 5D-F)**. Interestingly, we noticed that USP10 overexpression also partially restored TRPP2 protein itself. RT-qPCR analysis revealed no change in TRPP2 mRNA levels **(Fig. S2)**, and CHX chase assays showed no significant extension of TRPP2 half-life, suggesting that this effect occurs through a mechanism distinct from the

canonical USP10-mediated deubiquitination pathway. Taken together, these data indicate that TRPP2 recruits USP10 to deubiquitinate and stabilize PD-L1, whereas the reciprocal regulation of TRPP2 by USP10 occurs via a distinct mechanism.

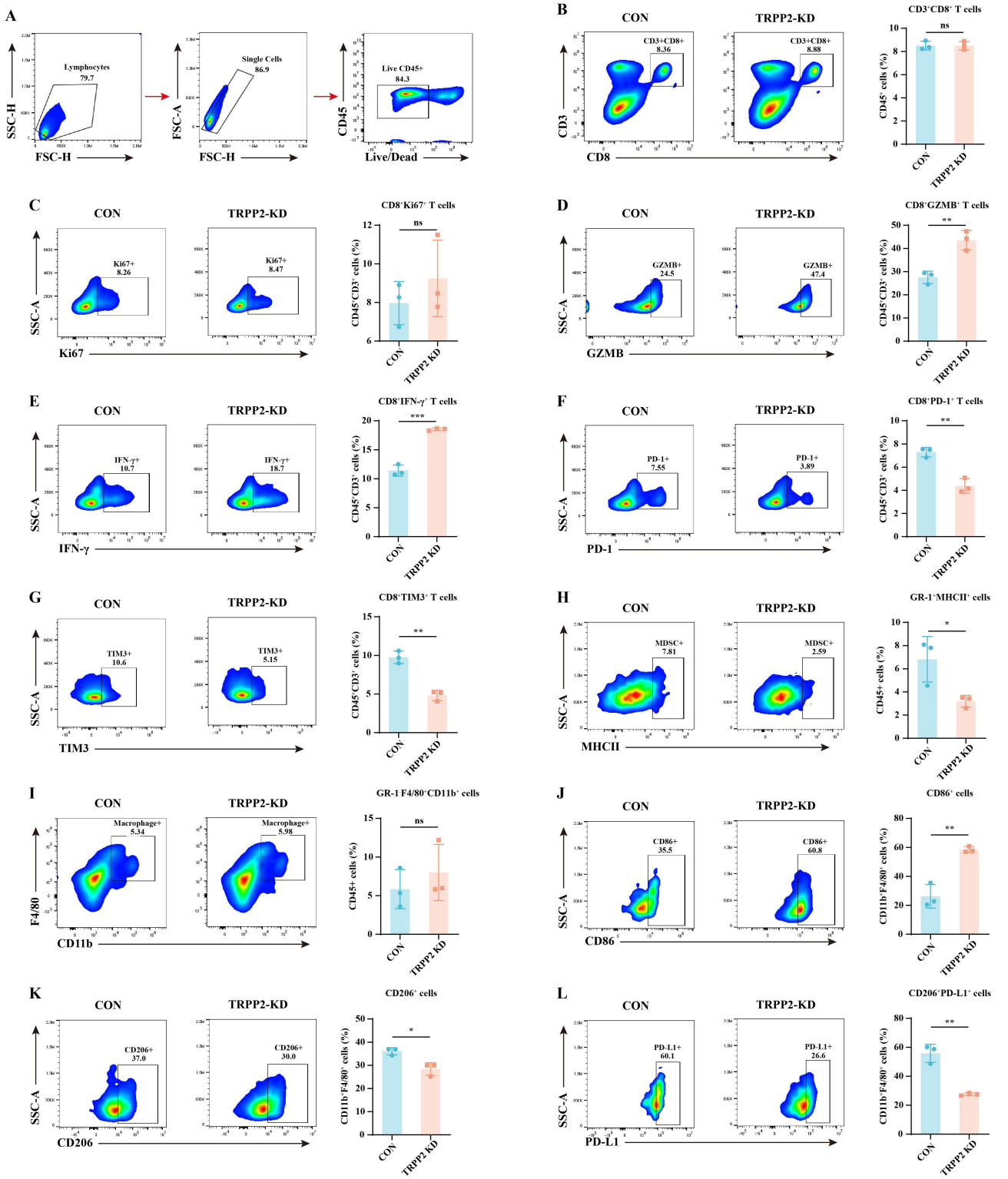


Figure 3. Silencing TRPP2 remodels the TIME by restoring CD8⁺T cell function and depleting immunosuppressive myeloid cells. (A) Gating strategy for identifying live leukocytes (Live⁺CD45⁺) within the TME. **(B-G)** Representative FC plots and statistical analyses of total CD8⁺T cell infiltration (CD3⁺CD8⁺), alongside their proliferative state (CD8⁺Ki67⁺), effector functions (CD8⁺GZMB⁺, CD8⁺IFN-γ⁺), and exhaustion status (CD8⁺PD-1⁺, CD8⁺TIM-3⁺). **(H-L)** Representative FC plots and quantification of MDSCs (GR-1⁺MHCII⁺), total TAMs (GR-1⁻CD11b⁺F4/80⁺), M1-type TAMs (CD11b⁺F4/80⁺CD86⁺), M2-type TAMs (CD11b⁺F4/80⁺CD206⁺), and PD-L1⁺M2 TAMs (CD11b⁺F4/80⁺CD206⁺PD-L1⁺) in control and TRPP2-knockdown tumors. **P*<0.05, ***P*<0.01 and ****P*<0.001. ns, not significant.

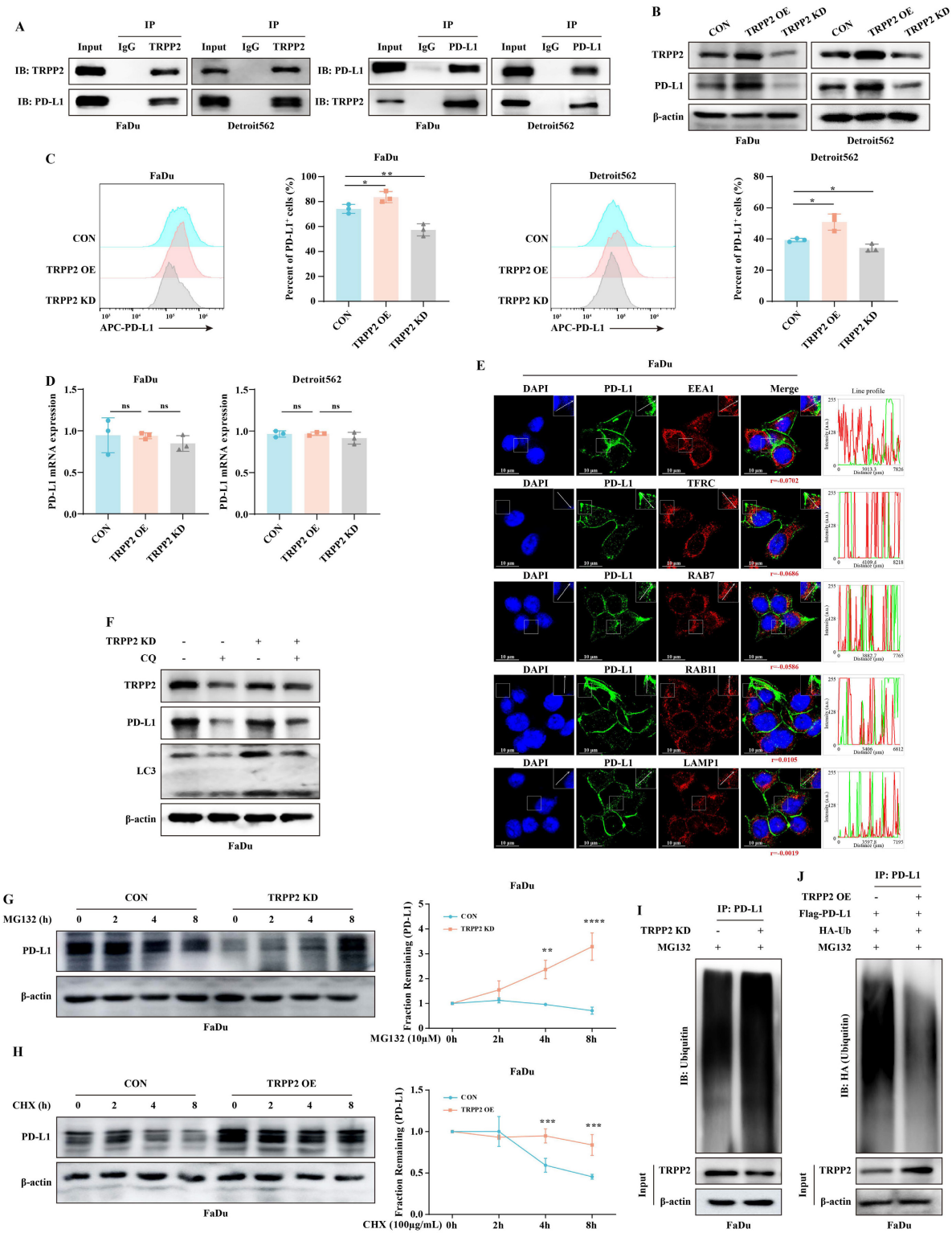


Figure 4. TRPP2 maintains intracellular PD-L1 abundance by preventing its proteasome-dependent degradation. (A) Co-IP assay detecting the physical interaction between endogenous TRPP2 and PD-L1 in HNC cells. **(B-C)** Evaluation of total cellular PD-L1 via western blotting and cell-surface PD-L1 via FC in HNC cells subjected to differential TRPP2 expression (knockdown or overexpression). **(D)** RT-qPCR analysis of PD-L1 mRNA levels, demonstrating no significant transcriptional regulation by TRPP2. **(E)** IF staining assessing the spatial relationship between PD-L1 and specific markers of the endocytic/lysosomal pathways (EEA1, TFRC, Rab7, Rab11, and LAMP1). **(F)** Western blotting showing the effect of the lysosomal inhibitor chloroquine (CQ, 10 μM) on PD-L1 and LC3 levels in control and TRPP2-knockdown cells. **(G)** Western blotting analysis of PD-L1 stability in control and TRPP2-KD cells treated with MG132 (10 μM) over an 8 h time course. For each individual time point, PD-L1 band intensities were first normalized to the β-actin loading control from the same time point and then normalized to the corresponding 0 h value (defined as 1). Group-by-time interaction: P=0.0003. **(H)** CHX (100 μg/mL) chase assay comparing PD-L1 protein half-life in control versus TRPP2-overexpressing (OE) cells. For each individual time point, PD-L1 band intensities were first normalized to the β-actin loading control from the same time point and then normalized to the corresponding 0 h value (defined as 1). Group-by-time: P=0.0006. **(I)** Ubiquitination assay detecting the polyubiquitination levels of endogenous PD-L1 in control and TRPP2-knockdown cells treated with MG132 for 8 h. **(J)** Ubiquitination assay of exogenous Flag-PD-L1 in control and TRPP2-overexpressing cells co-transfected with HA-Ub and treated with MG132. *P<0.05, **P<0.01, ***P<0.001 and ****P<0.0001. ns, not significant.

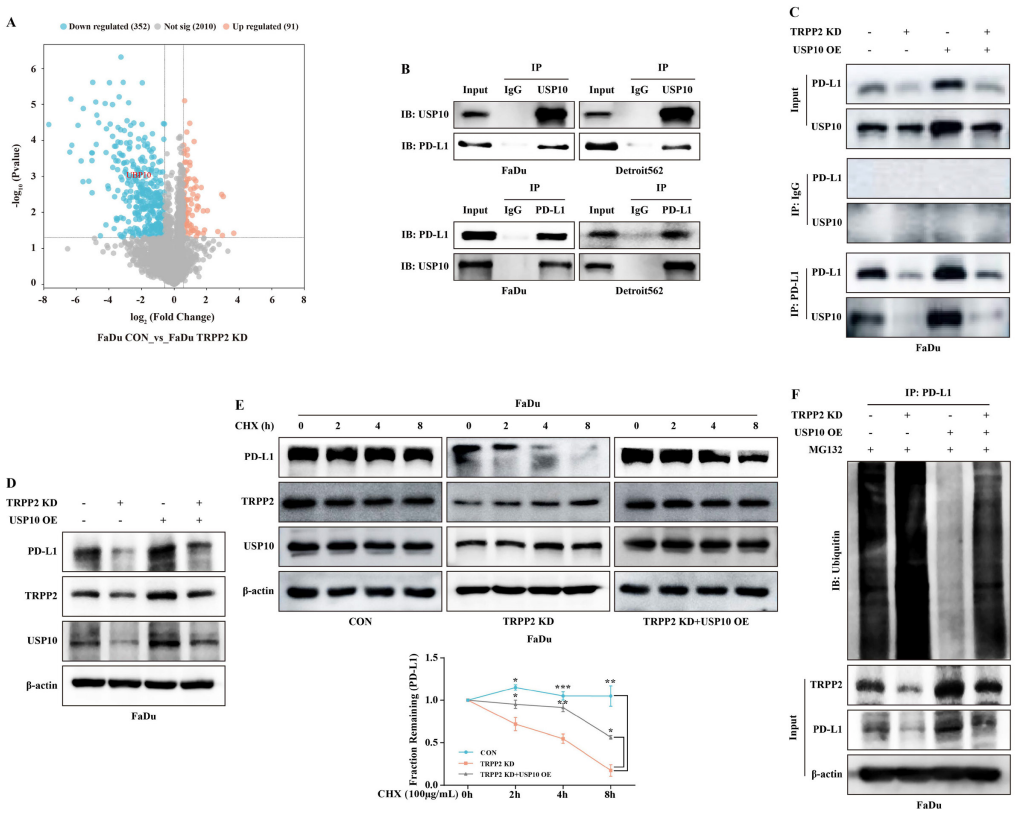


Figure 5. TRPP2 recruits the deubiquitinase USP10 to deubiquitinate and stabilize PD-L1. (A) Volcano plot of differentially expressed proteins in TRPP2-knockdown HNC cells, highlighting deubiquitinase candidates (Fold Change>1.5, $P<0.05$). **(B)** Co-IP assay confirming the interaction between endogenous USP10 and PD-L1 in HNC cells. **(C)** Co-IP assay confirming that TRPP2 knockdown attenuates the USP10-PD-L1 interaction in HNC cells. **(D)** Western blotting analysis demonstrating the rescue of PD-L1 expression by overexpressing USP10 in TRPP2-knockdown cells. **(E)** CHX chase assay (100 μg/mL, 0-8 h) assessing PD-L1 protein half-life in TRPP2-knockdown FaDu cells with or without USP10 overexpression. For each individual time point, PD-L1 band intensities were first normalized to the β-actin loading control from the same time point and then normalized to the corresponding 0 h value (defined as 1). Group-by-time interaction: $P<0.0001$, indicating that USP10 overexpression significantly restored PD-L1 stability in TRPP2-KD cells. **(F)** Ubiquitination assay showing that USP10 overexpression reverses the enhanced PD-L1 ubiquitination induced by TRPP2 silencing. *$P<0.05$, **$P<0.01$ and ***$P<0.001$.

TRPP2 endows exosomes with direct immunosuppressive capacity via membrane-bound PD-L1

In addition to stabilizing the intracellular PD-L1 pool, we hypothesized that HNC cells export this checkpoint molecule via exosomes to exert distal immunosuppressive effects. IF imaging and Pearson's correlation analysis revealed that TRPP2 overexpression significantly enhanced PD-L1 co-localization with the MVB marker CD63, whereas TRPP2 knockdown markedly reduced it **(Fig. 6A-B)**. Following successful isolation and characterization of HNC-derived exosomes **(Fig. 6C-F)**, we found by western blotting and ELISA that TRPP2 upregulation increased both soluble PD-L1 within the exosomal lumen **(Fig. 6G-H)** and membrane-bound PD-L1 exposed on the exosomal surface **(Fig. 6I-J)**. To determine whether this surface-exposed PD-L1 is functionally competent, we performed binding assays using recombinant human PD-1 protein. Exosomes derived from TRPP2-overexpressing cells exhibited significantly enhanced PD-1 binding capacity compared to those from control cells **(Fig. 6K-L)**. These results demonstrate that TRPP2 equips tumor-derived exosomes with the molecular machinery to act as mobile immunosuppressive decoys capable of directly engaging PD-1 on T cells.

TRPP2 drives the precise sorting of PD-L1 into exosomes via the ESCRT-0 component HRS

To identify the ESCRT machinery responsible for exosomal PD-L1 sorting, we first examined the expression of ESCRT-0 components (HRS and STAM) using the ENCORI database. The expression of HRS and STAM was positively correlated with TRPP2 in HNC tissues, with correlation coefficients of 0.246 and 0.387, respectively **(both $P < 0.05$; Fig. 7A-B)**. We then validated that TRPP2 regulates HRS, but not STAM, at the mRNA level in HNC cells **(Fig. 7C-D)**. Therefore, we focused on HRS. Co-IP assays confirmed the formation of a ternary complex comprising TRPP2, PD-L1, and HRS in HNC cells **(Fig. 7E)**. Consequently, TRPP2 overexpression increased both total HRS protein abundance and its spatial co-localization with PD-L1 **(Fig. 7F-H)**.

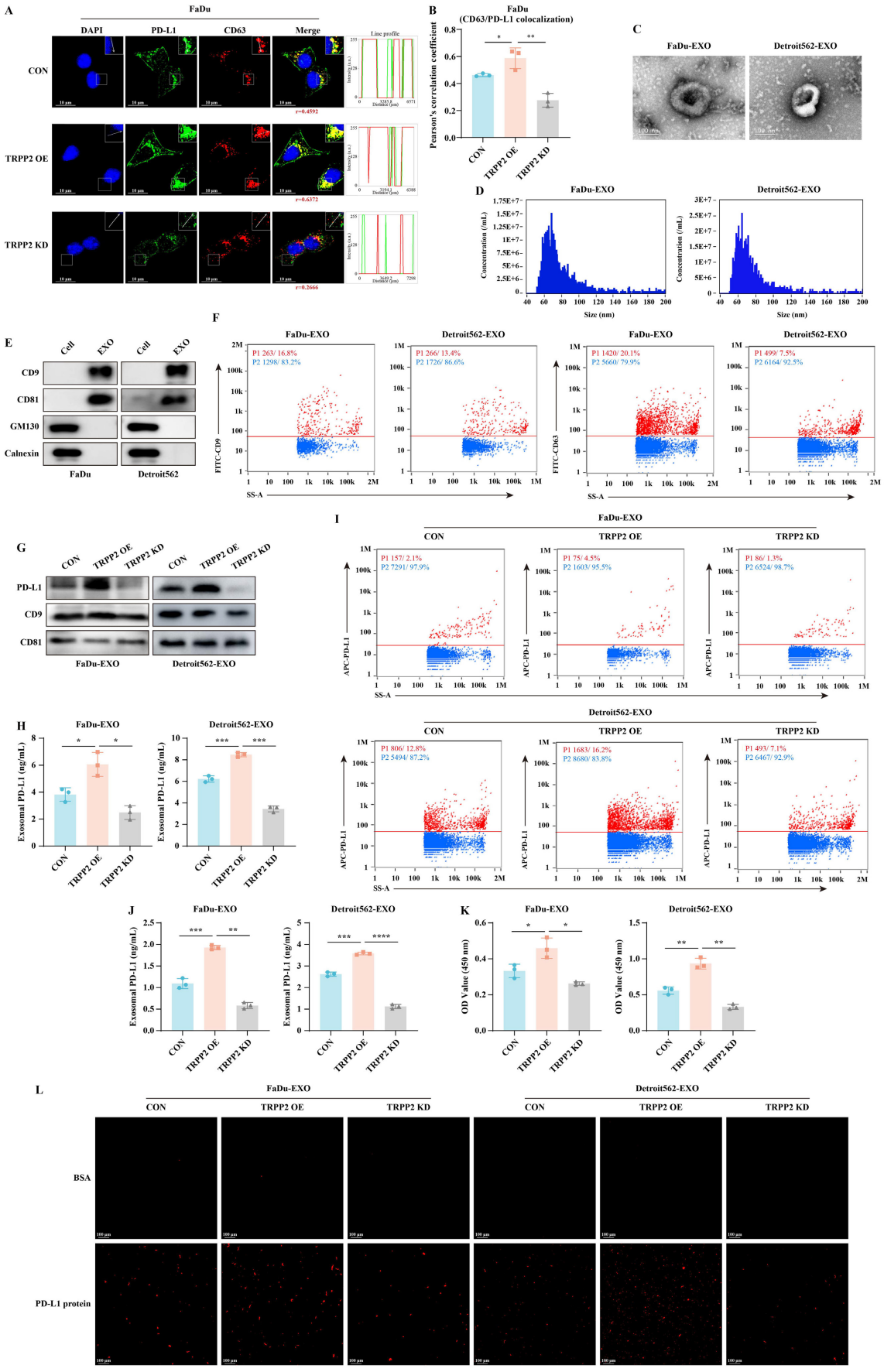


Figure 6. TRPP2 drives the secretion of exosomes enriched with functionally active membrane-bound PD-L1. (A) Representative IF images showing the intracellular co-localization of PD-L1 with the MVB marker CD63 in HNC cells with differential TRPP2 expression. **(B)** Quantification of Pearson's correlation coefficient for

PD-L1 and CD63 co-localization in HNC cells with differential TRPP2 expression. **(C-E)** Characterization of HNC-derived exosomes via TEM, NTA and western blotting. **(F)** Nanoscale flow cytometry validation of classic exosomal markers (CD9 and CD63). **(G-H)** Evaluation of soluble PD-L1 levels within the exosomal lumen using western blotting and ELISA under varying TRPP2 expression conditions. **(I-J)** Quantification of membrane-bound PD-L1 exposed on the intact exosomal surface via nanoscale flow cytometry and ELISA. **(K-L)** Binding assays evaluating the affinity between exosomal surface PD-L1 and recombinant human PD-1 protein, measured by ELISA and fluorescence imaging. **P*<0.05, ***P*<0.01, ****P*<0.001 and *****P*<0.0001.

To functionally validate the reliance of this axis on HRS, we silenced HRS using two independent siRNAs (siHRS#2 and siHRS#3; **Fig. 7I**). Notably, HRS depletion abolished the TRPP2-induced increase in intracellular PD-L1 and also reduced TRPP2 protein levels **(Fig. 7J)**. To determine whether this reduction occurred at the transcriptional level, we examined TRPP2 mRNA levels upon HRS knockdown. RT-qPCR analysis revealed that TRPP2 mRNA levels remained unchanged in TRPP2-overexpressing cells following HRS silencing **(Fig. S3)**, indicating that HRS does not affect TRPP2 transcription. This concurrent downregulation indicates a strong mutual dependency among the components of this ternary complex. It suggests that beyond its canonical role in vesicle sorting, HRS expression is essential for maintaining the overall stability of the TRPP2 and PD-L1 protein pool. Furthermore, IF staining and Pearson's correlation analysis confirmed that HRS knockdown significantly reduced PD-L1/CD63 co-localization in TRPP2-overexpressing cells **(Fig. 7K-L)**. Western blotting analysis showed that HRS silencing reduced the enrichment of PD-L1 and HRS in secreted exosomes **(Fig. 7M)**. Consistently, exosomes from TRPP2-knockdown cells also exhibited reduced levels of PD-L1 and HRS **(Fig. S4)**. These findings suggest that TRPP2 orchestrates the exosomal export of PD-L1 by transcriptionally upregulating HRS, which concurrently serves as a structural scaffold to maintain the stability of this sorting axis.

We next examined whether TRPP2's ion channel activity also contributes to PD-L1 regulation. Treatment with amiloride, a known TRPP2 channel blocker, resulted in a significant reduction in both cellular PD-L1 and exosomal PD-L1 levels, as well as a moderate decrease in HRS protein expression **(Fig. S5)**, suggesting that TRPP2's channel activity partially influences PD-L1 regulation and HRS expression. Collectively, these findings suggest that TRPP2 coordinates exosomal PD-L1 export by upregulating HRS, and that HRS exhibits a reciprocal dependency with TRPP2 at the protein level to maintain the stability of this sorting axis. Furthermore, TRPP2's ion channel activity partially contributes to PD-L1 regulation, supporting a dual-mechanism model involving both scaffolding function and channel activity.

Exosomal PD-L1 is internalized by macrophages to induce M2 polarization

Beyond direct engagement of T cells, PD-L1-enriched exosomes may re-educate other immune populations within the TME. *In vitro* tracking experiments confirmed that macrophages efficiently internalize PKH26-labeled HNC-derived exosomes **(Fig. 8A)**. Exosome uptake by macrophages did not differ between control and TRPP2-overexpressing groups, indicating that TRPP2 does not affect the efficiency of exosome internalization. FC analysis revealed that exosomes from TRPP2-knockdown cells failed to sustain PD-L1 expression on the surface of recipient macrophages **(Fig. 8B)**. To determine whether this surface PD-L1 transfer depends on active phagocytosis, macrophages were pretreated with Dynasore (80 μM), a dynamin inhibitor that blocks endocytic uptake, followed by co-incubation with exosomes for 48 h. FC analysis revealed that Dynasore treatment significantly attenuated the exosome-induced upregulation of surface PD-L1 on macrophages **(Fig. S6)**, indicating that the transfer of exosomal PD-L1 to recipient cell surface requires an active phagocytic process. Transcriptomic profiling of macrophages treated with exosomes derived from TRPP2-knockdown cells exhibited significant downregulation of gene sets associated with inflammatory responses and immune activation **(Fig. 8C-D)**. Phenotypically, exosomes generated from TRPP2-overexpressing cells robustly promoted M2-type features while suppressing M1 markers; conversely, exosomes from TRPP2-knockdown cells elicited the opposite polarization profile **(Fig. 8E-F)**. Furthermore, TRPP2-knockdown exosomes significantly reduced the emergence of the highly immunosuppressive PD-L1^{+}CD206^{+} double-positive macrophage population **(Fig. 8G)**. To establish whether the M2-polarizing effect was directly mediated by exosomal PD-L1, we performed a neutralizing antibody blockade assay. Macrophages were treated with TRPP2-overexpressing cell-derived exosomes in the presence of anti-PD-L1 antibody (10 μg/mL). Notably, anti-PD-L1 antibody treatment significantly attenuated exosome-induced M2 polarization and reduced the CD206^{+} macrophage population **(Fig. S7)**. These data delineate a secondary evasion mechanism wherein TRPP2-driven exosomal PD-L1 directly coerces macrophage polarization toward a pro-tumor M2 phenotype.

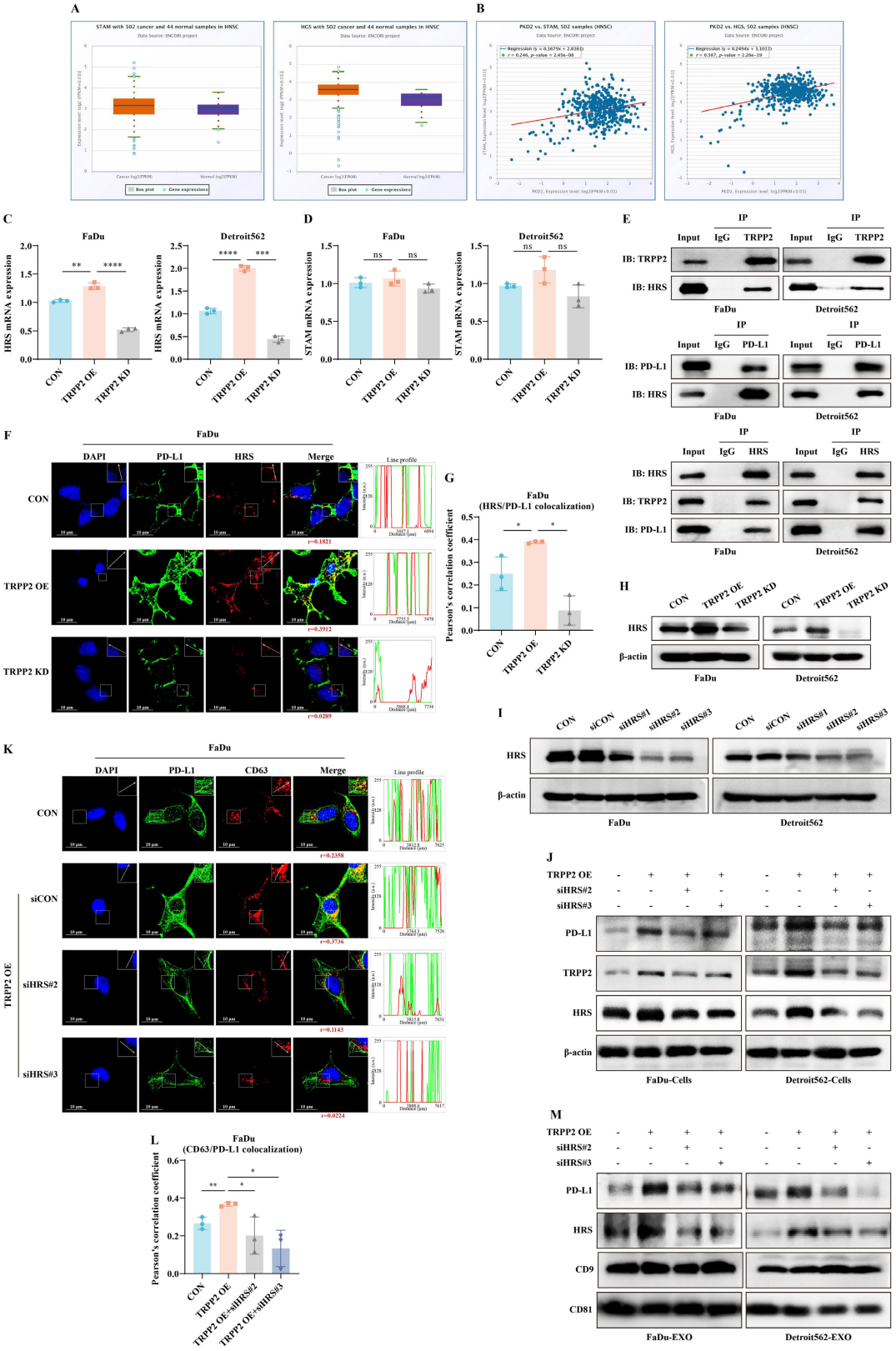


Figure 7. TRPP2 orchestrates the precise sorting of PD-L1 into exosomes via the ESCRT-0 component HRS. (A-B) Database analysis (ENCORI) detailing the expression levels of ESCRT-0 components (HRS and STAM) in HNC tissues and their positive correlation with TRPP2 expression. **(C-D)** RT-qPCR quantification of HRS and STAM mRNA levels in HNC cells following TRPP2 knockdown or overexpression. **(E)** Co-IP assay demonstrating the formation of a TRPP2-PD-L1-HRS ternary complex. **(F)** IF staining evaluating the spatial co-localization of PD-L1 and HRS. **(G)** Quantification of Pearson's correlation coefficients for PD-L1 and HRS co-localization in control versus TRPP2-overexpressing cells. **(H)** Western blotting was performed to detect total HRS protein levels following TRPP2 modulation. **(I)** Western blotting confirmation of HRS silencing efficiency using specific siRNAs. **(J-K)** Rescue experiments in TRPP2-overexpressing cells subjected to concomitant HRS silencing, assessing the intracellular accumulation of PD-L1 and HRS, the co-localization of PD-L1 with CD63. **(L)** Quantification of Pearson's correlation coefficients for PD-L1 and CD63 co-localization in TRPP2-overexpressing cells transfected with siCON or siHRS. **(M)** Western blotting analysis of the packaging levels of PD-L1 and HRS into secreted exosomes following concomitant HRS silencing in TRPP2-overexpressing cells. **P*<0.05, ***P*<0.01, ****P*<0.001 and *****P*<0.0001. ns, not significant.

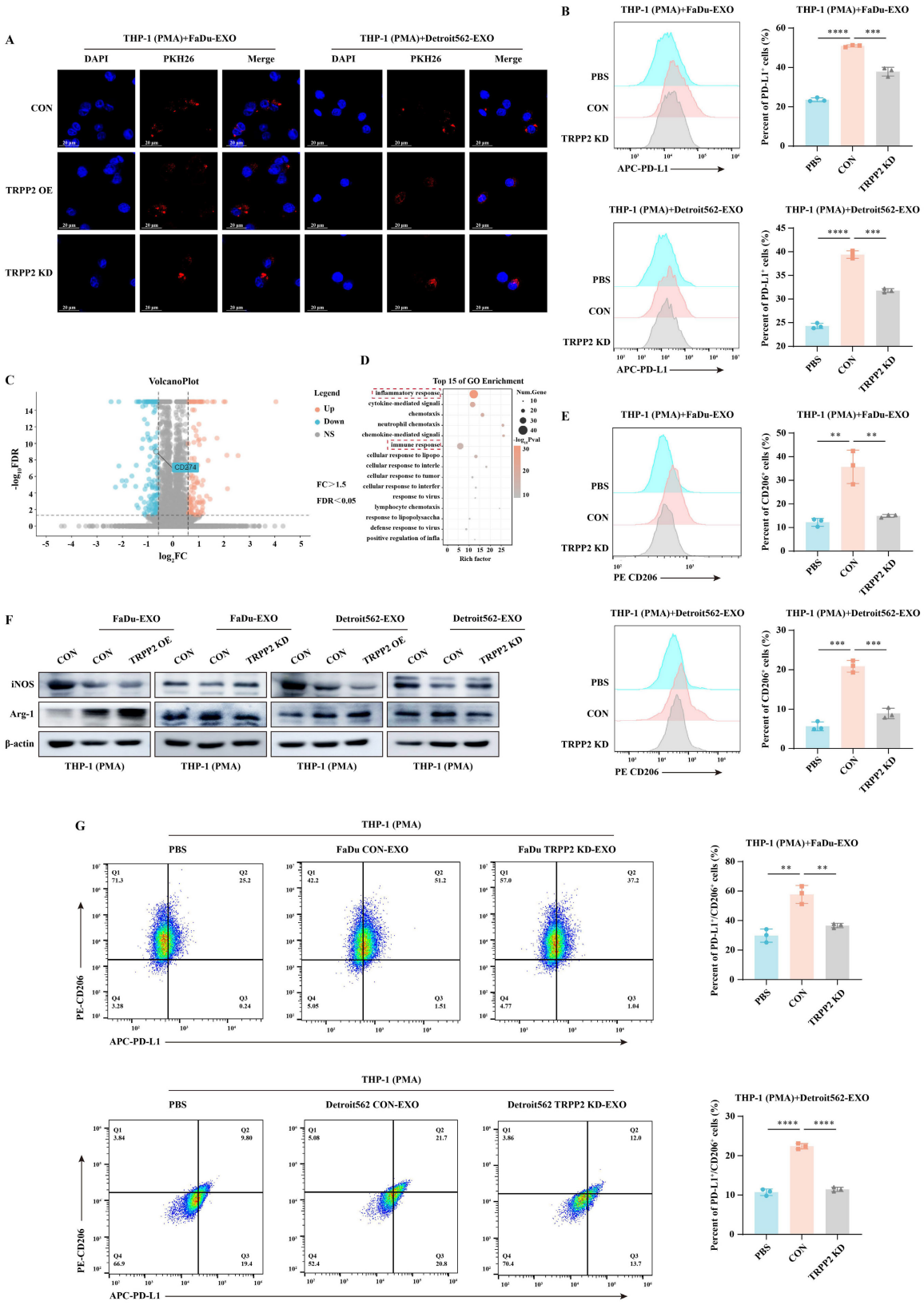


Figure 8. Exosomal PD-L1 derived from TRPP2-expressing cells promotes macrophage M2 polarization. (A) Fluorescence microscopy tracking the efficient internalization of PKH26-labeled HNC exosomes by recipient macrophages. **(B)** FC evaluating PD-L1 expression on the macrophage surface following incubation with exosomes derived from control or TRPP2-knockdown HNC cells. **(C-D)** Transcriptomic profiling of macrophages treated with TRPP2-knockdown exosomes, displayed as a volcano plot of differentially expressed genes and a bubble chart of enriched biological processes related to immune and inflammatory responses. **(E-F)** Phenotypic assessment of exosome-educated macrophages, analyzing the M2 marker CD206 via FC and the M1/M2 polarization markers (iNOS and Arg-1) via western blotting. **(G)** FC quantification of the highly immunosuppressive PD-L1^{+}/CD206^{+} double-positive macrophage population post-exosome treatment. Exosomes were normalized by total protein amount (BCA assay) before addition to cells. ***P*<0.01, ****P*<0.001 and *****P*<0.0001.

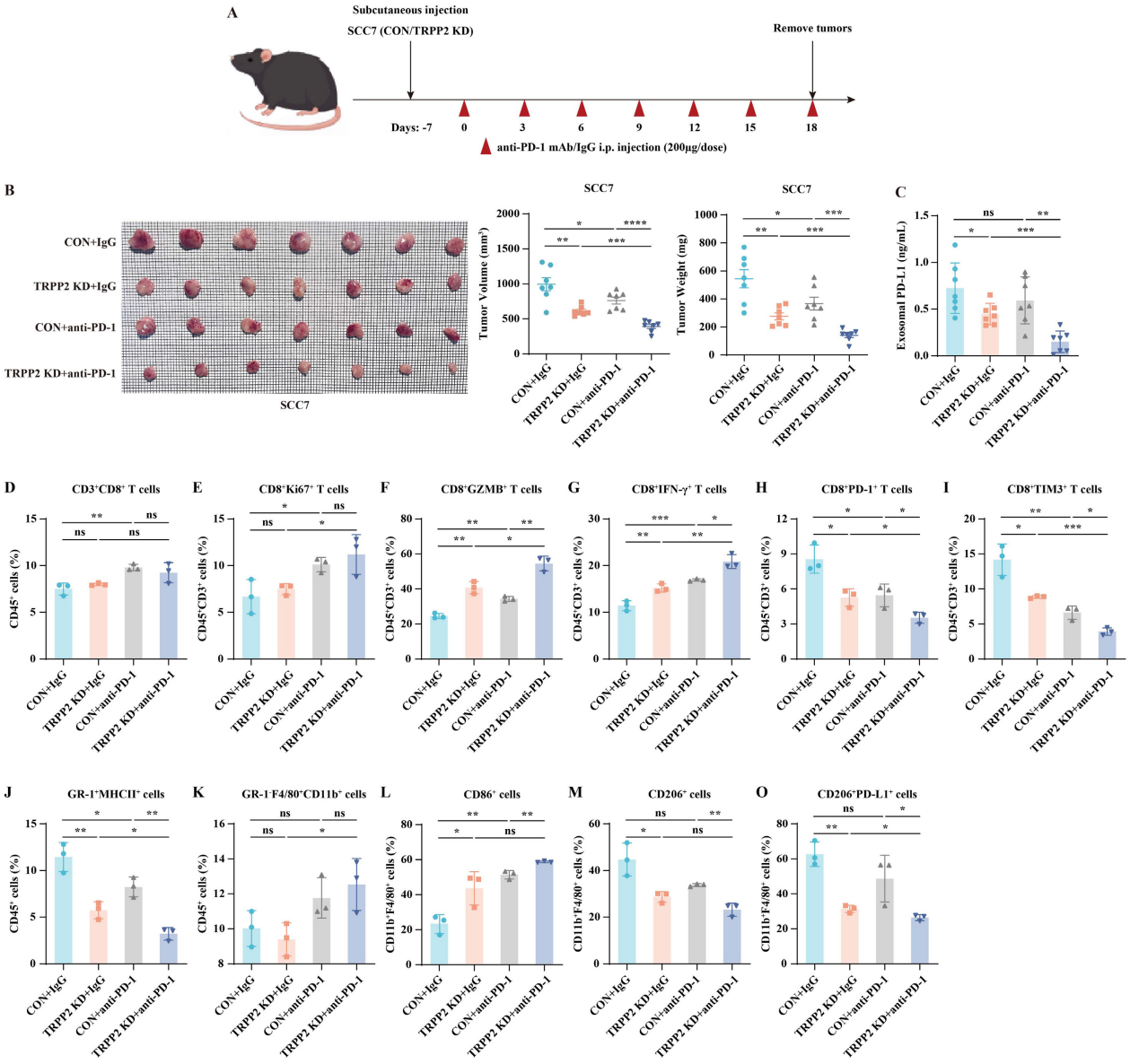


Figure 9. Targeting the TRPP2 axis synergistically sensitizes HNC to anti-PD-1 blockade therapy. (A) Schematic illustration of the subcutaneous tumor model establishment and the *in vivo* anti-PD-1 mAb treatment regimen. **(B)** Tumor growth curves (volume) and final tumor weights demonstrating the synergistic suppressive effect of combining TRPP2 knockdown with anti-PD-1 mAb therapy. **(C)** ELISA quantification of systemic PD-L1 levels in plasma-derived exosomes isolated from the treated mice. **(D-I)** Intratumoral FC profiling of the T cell compartment across experimental groups, analyzing total $CD8^+$T cells, proliferative capacity ($CD8^+Ki67^+$), effector functions ($CD8^+GZMB^+$, $CD8^+IFN\text{-}\gamma^+$), and exhaustion markers ($CD8^+PD\text{-}1^+$, $CD8^+TIM\text{-}3^+$). **(J-O)** FC analysis of the intratumoral myeloid compartment, detailing the infiltration of MDSCs ($GR\text{-}1^+MHCII^+$), total TAMs ($GR\text{-}1^-CD11b^+F4/80^+$), M1-type TAMs ($CD11b^+F4/80^+CD86^+$), M2-type TAMs ($CD11b^+F4/80^+CD206^+$), and PD-L1-expressing M2-type TAMs. **P*<0.05, ***P*<0.01, ****P*<0.001 and *****P*<0.0001. ns, not significant.

Targeting TRPP2 synergistically enhances the efficacy of anti-PD-1 mAb therapy in HNC

Having elucidated the dual TRPP2-USP10-PD-L1 (stability) and TRPP2-HRS-PD-L1 (sorting) regulatory axes, we evaluated the therapeutic potential of targeting this network *in vivo*. C3H mice bearing subcutaneous tumors were treated with either IgG or an anti-PD-1 mAb in the presence or absence of TRPP2 knockdown **(Fig. 9A)**. Whereas anti-PD-1 mAb exerted only modest tumor control, combination with TRPP2 depletion yielded a dramatic and synergistic suppression of both tumor volume and weight **(Fig. 9B)**. Notably, anti-PD-1 mAb alone failed to reduce PD-L1 levels in plasma-derived exosomes, but the combination strategy effectively depleted circulating exosomal PD-L1 **(Fig. 9C)**. Intratumoral FC analysis further revealed that combination therapy profoundly reduced exhausted $CD8^+PD\text{-}1^+$ and $CD8^+TIM\text{-}3^+$ T cells, as well as M2-type TAMs ($CD11b^+F4/80^+CD206^+$) and MDSCs ($GR\text{-}1^+MHCII^+$), while simultaneously driving an influx of effector $CD8^+GZMB^+$ and $CD8^+IFN\text{-}\gamma^+$ T cells **(Fig. 9D-O, Fig. S8)**. Histological examination of major organs (heart, liver, spleen, lung, kidney) revealed no overt

morphological abnormalities across treatment groups, and no significant body weight loss was observed in the combination group compared to controls, indicating a favorable biosafety profile **(Fig. S9)**. These translational findings demonstrate that silencing TRPP2 dismantles multiple layers of immune resistance, effectively sensitizing HNC to anti-PD-1 mAb therapy.

Discussion

Resistance to ICIs is a multifaceted process driven by tumor cell-intrinsic alterations and dynamic remodeling of the TIME [21, 22]. Although PD-1/PD-L1 inhibitors are approved for the treatment of HNC, the persistently low response rate remains a formidable clinical challenge. Most prior studies have focused on transcriptional regulation of PD-L1, whereas its post-translational stability and subcellular trafficking remain poorly understood [6, 23]. In this study, we identify the cation channel TRPP2 as a central hub that bridges these two levels of regulation: TRPP2 not only stabilizes intracellular PD-L1 via USP10-mediated deubiquitination, but also promotes its exosomal export through HRS upregulation, thereby establishing a dual-layer immunosuppressive barrier.

One principal finding of this work is that TRPP2 drives the aberrant intracellular accumulation of PD-L1. Having excluded transcriptional regulation and lysosomal degradation, we demonstrate that TRPP2 recruits the deubiquitinase USP10 to protect PD-L1 from proteasomal destruction. However, a critical question is how this intracellular PD-L1 reservoir contributes to systemic immune evasion. This prompted us to investigate a second, parallel mechanism involving TRPP2-mediated exosomal sorting via HRS. Canonically, the ESCRT-0 complex recognizes ubiquitinated cargo for lysosomal targeting or exosomal secretion [19, 24]. Notably, our data reveal that PD-L1 continues to be packaged into exosomes even after USP10-mediated deubiquitination. This observation implies that vesicle sorting in malignant cells exhibits considerable plasticity. We postulate that TRPP2-driven upregulation of HRS may promote the incorporation of PD-L1 into exosomes either through increased substrate availability (mass-action) or via recognition of a specific deubiquitinated conformation that circumvents the canonical requirement for ubiquitin tags. This model reconciles the seemingly paradoxical stabilization and secretion of PD-L1 and provides new insight into non-canonical sorting pathways operative in cancer. However, the detailed molecular basis by which HRS recognizes PD-L1, including the specific interaction domains and the potential role of post-translational modifications, remains to be determined in future studies. In this context, we also observed that HRS knockdown reduced TRPP2 protein levels without affecting its mRNA expression, suggesting a reciprocal stabilization between HRS and TRPP2 at the protein level. This mutual dependency further supports the notion that HRS functions beyond cargo sorting, serving as an integral component of the TRPP2-PD-L1-HRS protein complex.

A fundamental question arises: how does a cation channel such as TRPP2 orchestrate these complex protein-trafficking events? Emerging evidence suggests that ion channels in cancer frequently function beyond ion translocation, participating in inter-organellar communication and the assembly of macromolecular complexes [25]. Our Co-IP assays detected direct interactions of TRPP2 with PD-L1, USP10, and HRS, supporting a scaffolding role in nucleating the deubiquitination machinery and exosomal sorting complex. To further dissect the contribution of its channel activity, we employed the TRPP2 channel inhibitor amiloride. Notably, amiloride treatment partially reduced both cellular and exosomal PD-L1 levels, suggesting that TRPP2's ion channel activity also contributes to PD-L1 regulation, likely via calcium signaling-mediated effects on both exosome biogenesis and PD-L1 expression. Thus, we propose a dual-mechanism model in which TRPP2 regulates PD-L1 stability through both its structural scaffold function and its channel activity. This scaffolding function, distinct from its canonical ion-conducting role, underscores a broader impact of TRPP2 in tumor immunology than previously appreciated.

Exosomal PD-L1 has emerged as a critical driver of immunotherapy resistance, functioning as a mobile decoy that sequesters therapeutic antibodies and exhausts T cells at distal sites [11, 12, 26]. Recent studies have further elucidated the regulatory mechanisms underlying exosomal PD-L1 sorting, identifying key molecules such as Munc13-4 and MFGE8 that control PD-L1 incorporation into exosomes [27, 28]. Concurrently, TRP channels have been increasingly recognized for their roles in tumor immunity, with TRPM2 implicated in macrophage polarization and other TRP channels involved in exosome biogenesis [29-32]. Our findings add a new dimension to both fields by establishing a functional link between a TRP channel (TRPP2) and the ESCRT-dependent exosomal PD-L1 sorting machinery. Specifically, we demonstrate that TRPP2-driven exosomal PD-L1 suppresses anti-tumor immunity through two distinct modalities: direct engagement of PD-1 on $CD8^+$ T cells, and internalization by macrophages to drive M2 polarization. Together with these recent advances, our identification of the TRPP2-HRS axis reveals a

convergence of calcium signaling and ESCRT-dependent machinery that governs exosomal PD-L1 regulation, extending the current understanding of TRP channel function beyond ion conductance to protein trafficking and immune modulation.

Beyond its immunosuppressive function, circulating exosomal PD-L1 holds translational potential as a non-invasive predictive biomarker for anti-PD-1 therapy response. In our study, plasma-derived exosomal PD-L1 levels were effectively reduced upon TRPP2 knockdown in combination with anti-PD-1 therapy, raising the possibility that dynamic monitoring could serve as an early indicator of therapeutic efficacy. This observation is particularly relevant given the accessibility of peripheral blood sampling, which allows for repeated, real-time monitoring of treatment response without the need for invasive tumor biopsies. While the clinical utility of exosomal PD-L1 as a biomarker has been demonstrated in melanoma [8], its application in HNC, particularly regarding sampling timing, selection of exosomal PD-L1 fractions, and standardization of detection protocols, remains to be further validated. Nevertheless, our findings provide a strong rationale for future clinical investigations to evaluate whether circulating exosomal PD-L1 levels, alone or in combination with other circulating biomarkers, could improve patient stratification and guide individualized immunotherapy in HNC.

Therefore, our findings highlight a promising translational strategy to circumvent immunotherapy resistance in HNC. Whereas conventional anti-PD-1 monotherapy is frequently undermined by the persistent decoy effect of circulating exosomal PD-L1, our source-to-sink approach offers a means to dismantle this systemic immunosuppressive barrier. By targeting the TRPP2 axis, we can simultaneously deplete the intracellular PD-L1 reservoir and sever the exosomal supply line. This dual-action strategy not only restores the functional competence of intratumoral $CD8^+$T cells but also prevents the re-education of the myeloid compartment, particularly the polarization of TAMs toward the M2 phenotype. Given that TRPP2 represents a therapeutic target with translational potential, the development of specific small-molecule inhibitors or the application of genetic interference strategies in conjunction with ICIs could substantially improve therapeutic outcomes for HNC patients who are refractory to current standard-of-care immunotherapies.

Conclusion

In summary, this study identifies a molecular cascade where TRPP2 coordinates the intracellular stability and extracellular sorting of PD-L1 in HNC. By acting as a scaffold protein, TRPP2 recruits USP10 to safeguard PD-L1 from proteasomal degradation. Furthermore, TRPP2-driven upregulation of HRS facilitates the precise packaging of this stabilized PD-L1 into exosomes. These exosomes act as potent systemic suppressors that directly exhaust $CD8^+$T cells and polarize macrophages toward a pro-tumor M2 phenotype. Our results define TRPP2 as a master regulator of immune evasion and establish a strong theoretical foundation for targeting the TRPP2-PD-L1 axis to sensitize HNC to immunotherapy. We acknowledge that the subcutaneous SCC7 syngeneic model, while widely used for immunotherapy studies, does not fully recapitulate the complex orthotopic microenvironment of human HNC, including anatomical location-specific immune interactions and stromal components. Future studies using orthotopic models and patient-derived xenografts (PDX) are warranted to further validate the translational potential of targeting the TRPP2-PD-L1 axis.

Supplementary Material

Supplementary figures and tables.
https://www.ijbs.com/v23p0059s1.pdf

Acknowledgements

This work was supported by Guangdong Basic Research Center of Excellence for Aggregate Science.

Funding

The study was supported by grants from the National Natural Science Foundation of China (Nos.82273391 and 82303444), China Postdoctoral Science Foundation (No. 2025M772168), Natural Science Foundation of Shenzhen Municipality (No. JCYJ20240813113556071) and 1+1+1 CUHK-CUHK(SZ)-GDSTC Joint Collaboration Fund (No. 2025A0505000064).

Author contributions

J.D. and Z.M. designed the experiments. Z.M. performed the statistical analyses. X.J. performed IHC scoring and data analysis. Z.M., J.W., J.S., Y.Z. and X.Z. conducted the experiments. X.H., S.B. and M.W. verified the authenticity of all raw data. Z.M. wrote the manuscript. J.D., Z.Y. and X.Y. revised the manuscript. All authors read and approved of the final manuscript.

Data availability

The raw data supporting the conclusions of this article, including proteomics and transcriptomics datasets, are available from the corresponding author upon reasonable request.

Ethics approval and consent to participate

Human HNC tissue samples were obtained from the First Affiliated Hospital of China Medical University with approval from the Ethics Committee of the First Affiliated Hospital of China Medical University (Approval No. 2026-4-2). Written informed consent was obtained from all patients. A total of 20 paired HNC and adjacent normal tissues were used in this study. All animal experiments were approved by the Animal Ethics Committee of the Chinese University of Hong Kong, Shenzhen (Approval No. CUHKSZ-AD-20250075). All experiments were performed in accordance with the committee's guidelines.

Competing Interests

The authors have declared that no competing interest exists.

References

1. Chikuie N, Urabe Y, Ueda T, Hamamoto T, Taruya T, Kono T, et al. Utility of plasma circulating tumor DNA and tumor DNA profiles in head and neck squamous cell carcinoma. Sci Rep. 2022;12:9316. doi: 10.1038/s41598-022-13417-5.
2. Liu C, Li M, Liu X, Shi T, Wang Y, Sui C, et al. Evaluating the efficacy and safety of different neoadjuvant immunotherapy combinations in locally advanced HNSCC: a systematic review and meta-analysis. Front Immunol. 2024;15:1467306. doi: 10.3389/fimmu.2024.1467306.
3. Lin C, Chu Y, Zheng Y, Gu S, Hu Y, He J, et al. Macrophages: plastic participants in the diagnosis and treatment of head and neck squamous cell carcinoma. Front Immunol. 2024;15:1337129. doi: 10.3389/fimmu.2024.1337129.
4. Sharon S, Bell RB. Immunotherapy in head and neck squamous cell carcinoma: a narrative review. Front Oral Maxillofac Med. 2022;4:48. doi: 10.21037/fomm-21-48.
5. Ruffin AT, Li H, Vujanovic L, Zandberg DP, Ferris RL, Bruno TC. Improving head and neck cancer therapies by immunomodulation of the tumour microenvironment. Nat Rev Cancer. 2023;23:173-188. doi: 10.1038/s41568-022-00531-9.
6. Yi M, Niu M, Xu L, Luo S, Wu K. Regulation of PD-L1 expression in the tumor microenvironment. J Hematol Oncol. 2021;14:10. doi: 10.1186/s13045-020-01027-5.
7. Wu Y, Fu H, Hao J, Yang Z, Qiao X, Li Y, et al. Tumor-derived exosomal PD-L1: a new perspective in PD-1/PD-L1 therapy for lung cancer. Front Immunol. 2024;15:1342728. doi: 10.3389/fimmu.2024.1342728.
8. Chen G, Huang AC, Zhang W, Zhang G, Wu M, Xu W, et al. Exosomal PD-L1 contributes to immunosuppression and is associated with anti-PD-1 response. Nature. 2018;560(7718):382-386. doi: 10.1038/s41586-018-0392-8.
9. Kuang L, Wu L, Li Y. Extracellular vesicles in tumor immunity: mechanisms and novel insights. Mol Cancer. 2025;24(1):45. doi: 10.1186/s12943-025-02233-w.
10. Guo X, Gao C, Yang DH, Li S. Exosomal circular RNAs: A chief culprit in cancer chemotherapy resistance. Drug Resist Updat. 2023;67:100937. doi: 10.1016/j.drup.2023.100937.
11. Li H, Chen X, Zheng S, Han B, Zhang X, Zheng X, et al. The expansion of MDSCs induced by exosomal PD-L1 promotes the progression of gastric cancer. J Transl Med. 2024;22:821. doi: 10.1186/s12967-024-05611-y.
12. Liu N, Zhang J, Yin M, Liu H, Zhang X, Li J, et al. Inhibition of xCT suppresses the efficacy of anti-PD-1/L1 melanoma treatment through exosomal PD-L1-induced macrophage M2 polarization. Mol Ther. 2021;29:2321-2334. doi: 10.1016/j.ymthe.2021.03.013.
13. Lu MM, Yang Y. Exosomal PD-L1 in cancer and other fields: recent advances and perspectives. Front Immunol. 2024;15:1395332. doi: 10.3389/fimmu.2024.1395332.
14. Koulen P, Cai Y, Geng L, Maeda Y, Nishimura S, Witzgall R, et al. Polycystin-2 is an intracellular calcium release channel. Nat Cell Biol. 2002;4:191-7. doi: 10.1038/ncb754.
15. Li K, Chen L, Lin Z, Zhu J, Fang Y, Du J, et al. Role of the AMPK/ACC Signaling Pathway in TRPP2-Mediated Head and Neck Cancer Cell Proliferation. Biomed Res Int. 2020;2020:4375075. doi: 10.1155/2020/4375075.
16. Gargalionis AN, Korkolopoulou P, Farmaki E, Piperi C, Dalagiorgou G, Adamopoulos C, et al. Polycystin-1 and polycystin-2 are involved in the acquisition of aggressive phenotypes in colorectal cancer. Int J Cancer. 2015;136(7):1515-27. doi: 10.1002/ijc.29140.
17. Messenger SW, Woo SS, Sun Z, Martin TFJ. A Ca^{2+}-stimulated exosome release pathway in cancer cells is regulated by Munc13-4. J Cell Biol. 2018;217:2877-2890. doi: 10.1083/jcb.201710132.
18. Alam MR, Rahman MM, Li Z. The link between intracellular calcium signaling and exosomal PD-L1 in cancer progression and immunotherapy. Genes Dis. 2023;11(1):321-334. doi: 10.1016/j.gendis.2023.01.026.
19. Henne WM, Buchkovich NJ, Emr SD. The ESCRT pathway. Dev Cell. 2011;21(1):77-91. doi: 10.1016/j.devcel.2011.05.015.
20. Quinney KB, Frankel EB, Shankar R, Kasberg W, Luong P, Audhya A. Growth factor stimulation promotes multivesicular endosome biogenesis by prolonging recruitment of the late-acting ESCRT machinery. Proc Natl Acad Sci U S A. 2019;116(14):6858-6867. doi: 10.1073/pnas.1817898116.
21. Sharma P, Hu-Lieskovan S, Wargo JA, Ribas A. Primary, Adaptive, and Acquired Resistance to Cancer Immunotherapy. Cell. 2017;168(4):707-723. doi: 10.1016/j.cell.2017.01.017.
22. Yang J, Tang S, Saba NF, Shay C, Teng Y. Tumor secretome shapes the immune landscape during cancer progression. J Exp Clin Cancer Res. 2025;44(1):47. doi: 10.1186/s13046-025-03302-0.
23. Zhou YJ, Li G, Wang J, Liu M, Wang Z, Song Y, et al. PD-L1: expression regulation. Blood Sci. 2023;5:77-91. doi: 10.1097/BS9.0000000000000149.
24. Lee YJ, Shin KJ, Jang HJ, Ryu JS, Lee CY, Yoon JH, et al. GPR143 controls ESCRT-dependent exosome biogenesis and promotes cancer metastasis. Dev Cell. 2023;58:320-334.e8. doi: 10.1016/j.devcel.2023.01.006.
25. Carpanese V, Festa M, Prosdocimi E, Bachmann M, Sadeghi S, Bertelli S, et al. Interactomic exploration of LRRC8A in volume-regulated anion channels. Cell Death Discov. 2024;10(1):299. doi: 10.1038/s41420-024-02032-0.
26. Yin Z, Yu M, Ma T, Zhang C, Huang S, Karimzadeh MR, et al. Mechanisms underlying low-clinical responses to PD-1/PD-L1 blocking antibodies in immunotherapy of cancer: a key role of exosomal PD-L1. J Immunother Cancer. 2021;9(1):e001698. doi: 10.1136/jitc-2020-001698.
27. Liu C, Liu D, Zheng X, Guan J, Zhou X, Zhang H, et al. Munc13-4 mediates tumor immune evasion by regulating the sorting and secretion of PD-L1 via exosomes. Nat Commun. 2025;16(1):9080. doi: 10.1038/s41467-025-64149-9.
28. Wang W, Chen J, Wang S, Sun X, Yang J, Yu P, et al. MFGE8 induces anti-PD-1 therapy resistance by promoting extracellular vesicle sorting of PD-L1. Cell Rep Med. 2025;6(2):101922. doi: 10.1016/j.xcrm.2024.101922.
29. Huang W, Wu Y, Luo N, Shuai X, Guo J, Wang C, et al. Identification of TRPM2 as a prognostic factor correlated with immune infiltration in ovarian cancer. J Ovarian Res. 2023;16(1):169. doi: 10.1186/s13048-023-01225-y.
30. Zheng D, Long S, Xi M. Identification of TRPM2 as a Potential Therapeutic Target Associated with Immune Infiltration: A Comprehensive Pan-Cancer Analysis and Experimental Verification in Ovarian Cancer. Int J Mol Sci. 2023;24(15):11912. doi: 10.3390/ijms241511912.
31. Kim MS, Yang SH, Kim MS. TRPML3 enhances drug resistance in non-small cell lung cancer cells by promoting Ca^{2+}-mediated lysosomal trafficking. Biochem Biophys Res Commun. 2022;627:152-159. doi: 10.1016/j.bbrc.2022.08.051.
32. Padbury EH, Bálint Š, Carter DRF, Becker EBE. TRPC3 signalling contributes to the biogenesis of extracellular vesicles. J Extracell Biol. 2023;3(1):e132. doi: 10.1002/jex2.70070.